Jour. Korean Inst. Mining Geol.
Vol. 19, No. 4, p. 283-292, 1986

Two-Dimensional Resistivity Modeling by Finite Element Method

Hee Joon Kim*

Abstract: Finite element method with linear triangular and bilinear rectangular elements is applied to solve the three-dimensional potential distribution due to a point source of current located in or on the surface of the earth containing arbitrary two-dimensional resistivity distribution. The modeling technique developed in this paper is flexible to model conductive inhomogeneity and surface topographies, and more accurate to evaluate surface potentials than the conventional techniques using finite difference method. Since it is possible to reduce nodal points with acceptable accuracy, this modeling technique is very efficient and economic in terms of execution time and core space. A few geologic structures adequate to demonstrate above features are simulated in this paper.

INTRODUCTION

The recent developments of data acquisition techniques with high accuracy and substantially higher rates over larger areas warrant a more sophisticated interpretation of the geologic structure. In regions such as sedimentary basins where the subsurface structure is approximately horizontal and the lateral variation is slow, a reasonable interpretation can be made by fitting layered (or one-dimensional) earth models. However, in many cases the structure is not layered. A more general interpretation assumes that regional resistivity varies little in strike direction. This is two-dimensional (2D) problem.

Finite element method (FEM) is a widely accepted numerical procedure for solving the differential equations in engineering and physics. The FEM can be easily applied to irregular-shaped objects composed of several different materials and having mixed boundary condition. These features of FEM are suitable to model 2D resistivity problems (Coggon, 1971; Fox *et al.*, 1980; Sasaki, 1981).

In this paper, the FEM is employed to solve the potential distribution due to a point source in or on the surface of the earth containing arbitrary 2D resistivity distribution. The FEM modeling technique has both linear triangular and bilinear rectangular elements. Although the rectangular element requires a specific coordinates, this property is not inconvenient in the resistivity modeling. Because of this specific coordinate, it is more efficient in constructing matrix equation than the triangular element. A great geometric flexibility of FEM, however, is derived from the triangular element. By using these elements, homogeneous half-space, dip and valley structures are simulated in this paper. A comparison between FEM and finite difference method (FDM) is carried out in the process of these simulations.

* Department of Applied Geology, National Fisheries University of Pusan

ENERGY MINIMIZATION

Electromagnetic fields behave in such a way that total energy is minimized. The FEM of calculating potentials and fields uses this principle directly.

For direct current, it is convenient to use scalar electric potentials. If a potential ϕ is generated by a point source with a strength of I located at the origin of Cartesian coordinate,

then the functional f corresponding to the total energy of the system is given by (Coggon, 1971)

$$f=\frac{1}{2}\iiint_V[\sigma(\nabla\phi)^2+2\phi I\delta(x)\delta(y)\delta(z)]\,dxdydz, \quad (1)$$

where σ is the conductivity of the earth and δ denotes the Dirac delta function.

If we assume that there are no changes in the conductivity distribution in y (strike) direction, *i.e.*,

$$\frac{\partial}{\partial y}[\sigma(x,y,z)]=0, \quad (2)$$

then the potential $\phi(x,y,z)$ is symmetric about $y=0$. Thus the Fourier cosine transform can be applied and

$$\Phi(x,g,y)=\int_0^\infty \phi(x,y,z)\cos(gy)\,dy, \quad (3)$$

where $\Phi(x,g,z)$ is the Fourier transformed potential. In this case, the functional f in (x, g, z) space equivalent to (1) is

$$f=\frac{1}{2}\iint_A\left\{\sigma\left[\left(\frac{\partial\Phi}{\partial x}\right)^2+g^2\Phi^2+\left(\frac{\partial\Phi}{\partial z}\right)^2\right]+2\Phi I\delta(x)\delta(z)\right\}dxdz. \quad (4)$$

The integration in (4) is carried over an area instead of a volume. However, inverse Fourier transformation is needed to obtain a potential ϕ.

FINITE ELEMENT METHOD

Let us divide a domain of interest into linear triangular and bilinear rectangular elements and consider the element equation.

In the linear triangular element, the nodes are labeled i, j and k. The nodal values of Φ at the nodal coordinates (x_i, z_i), (x_j, z_j) and (x_k, z_k) are Φ_i, Φ_j and Φ_k, respectively. By expressed I by a linear equation in the interior of the triangular element, the element equation becomes (Appendix)

$$\frac{\sigma}{4a}\begin{bmatrix} b_i & c_i \\ b_j & c_j \\ b_k & c_k \end{bmatrix}\begin{bmatrix} b_i b_j b_k \\ c_i c_j c_k \end{bmatrix}\begin{bmatrix}\Phi_i\\ \Phi_j\\ \Phi_k\end{bmatrix}+\frac{\sigma g^2 A}{12}\begin{bmatrix}2&1&1\\1&2&1\\1&1&2\end{bmatrix}\begin{bmatrix}\Phi_i\\ \Phi_j\\ \Phi_k\end{bmatrix}+I_n\begin{bmatrix}\delta_i\\ \delta_j\\ \delta_k\end{bmatrix}=0 \quad (5)$$

where

$$A=\frac{1}{2}\begin{bmatrix}1&x_i&z_i\\1&x_j&z_j\\1&x_k&z_k\end{bmatrix},$$

$b_i=z_j-z_k$, $b_j=z_k-z_i$, $b_k=z_i-z_j$,

$c_i=x_k-x_j$, $c_j=x_i-x_k$, $c_k=x_j-x_i$,

I_n is the total current supplied in the element, and δ_n $(n=i, j$ or $k)=1$ for the case that n is located at the origin and $\delta_n=0$ for the other cases.

In the bilinear rectangular element, on the other hand, the nodes are labeled i, j, k and m. The nodal values at the nodal coordinates (x_i, z_i), (x_j, z_j), (x_k, z_k) and (x_m, z_m) are Φ_i, Φ_j, Φ_k and Φ_m, respectively. The element equation for the rectangular element is (Appendix)

$$\frac{\sigma a}{6b}\begin{pmatrix}2&-2&-1&1\\-2&2&1&-1\\-1&1&2&-2\\1&-1&-2&2\end{pmatrix}\begin{pmatrix}\Phi_i\\ \Phi_j\\ \Phi_k\\ \Phi_m\end{pmatrix}+\frac{\sigma b}{6a}\begin{pmatrix}2&1&-1&-2\\1&2&-2&-1\\-1&-2&2&1\\-2&-1&1&2\end{pmatrix}\begin{pmatrix}\Phi_i\\ \Phi_j\\ \Phi_k\\ \Phi_m\end{pmatrix}+\frac{\sigma g^2 ab}{9}\begin{pmatrix}4&2&1&2\\2&4&2&1\\1&2&4&2\\2&1&2&4\end{pmatrix}\begin{pmatrix}\Phi_i\\ \Phi_j\\ \Phi_k\\ \Phi_m\end{pmatrix}+I_n\begin{pmatrix}\delta_i\\ \delta_j\\ \delta_k\\ \delta_m\end{pmatrix}=0, \quad (6)$$

where

$a=y_m-y_i$, and $b=x_j-x_i$.

Assembling (5) and (6) for all elements and introducing the boundary conditions produce a matrix equation

$$[\underline{K}]\ \underline{P}=\underline{S}, \quad (7)$$

where $[\underline{K}]$ is the coefficient matrix of order n (n is the number of nodal points), $\underline{P}$ the column vector of Φ_i $(i=1, 2, \ldots, n)$ and $\underline{S}$ the column

vector about current sources. The matrix $[\underline{K}]$ is always symmetric and positive definite, and the diagonal coefficients, K_{ii}, are always positive and relatively large when compared to the off-diagonal values in the same row. The relatively large diagonal coefficient allows Gaussian elimination to be performed without interchanging rows (pivoting). This is an important fact because only the non-zero coefficients need to be stored within the computer. The symmetric property is also important because there is no need to store the coefficients below the main diagonal. In this study, (7) is solved by a modified Gaussian elimination method (Conte and deBoor, 1980).

POTENTIAL ESTIMATION

In order to calculate the inverse Fourier transform and to obtain the potential ϕ, the matrix inversion of (7) must be carried out for various values of g. From (3), the potential to be estimated is

$$\phi(x, 0, z)=\frac{2}{\pi}\int_0^{\infty}\Phi(x, g, z)\ dg. \qquad (8)$$

Since Φ generally decreases monotonically to zero as $g\rightarrow\infty$, the numerical integration of (8) is easy to perform with an adequate sampling. In this study, the numerical integration is carried out by fitting the envelope of Φ in each subsection $g_1 \leqslant g \leqslant g_2$ by an exponential function of $a\cdot\exp(-bg)$ and using an analytic form

$$\int_{g_1}^{g_2} a\ e^{-bg}\ dg=\frac{1}{b}[\Phi(g_1)-\Phi(g_2)], \qquad (9)$$

and then taking the cumulative sum of these subsectional integrals up to reasonably large values of g.

NUMERICAL RESULTS

A few examples of resistivity modeling indicate the versatility of the FEM described in the previous sections. First of all to estimate the accuracy of the FEM, a homogeneous earth of 100 $\Omega\cdot$m was simulated. Its model, which consists of only bilinear rectangular elements, has a grid of 53×12 (=636) nodes (Fig. 1).

Fig. 2 shows the Fourier transformed potential Φ as a function of wavenumber g due to a point source. The numerical solutions are slightly smaller than the corresponding analytic solutions because of errors associated with numerical approximations. The error is more apparent in small wavenumber region, but fortunately this does not give a significant contribution in the numerical integration. Fig. 3 shows the surface potentials due to a point source. The FEM solution is slightly smaller than an analytic one because the transformed potential undershoots as

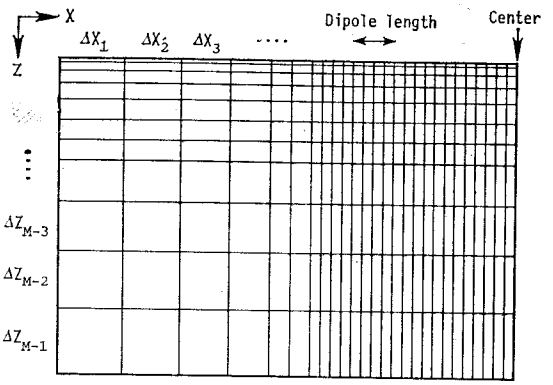

Fig. 1 Left half of rectangular grid.

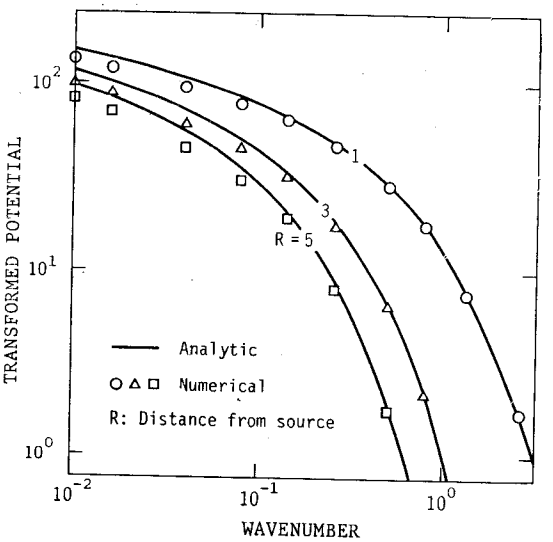

Fig. 2 Fourier transformed potentials due to a point source.

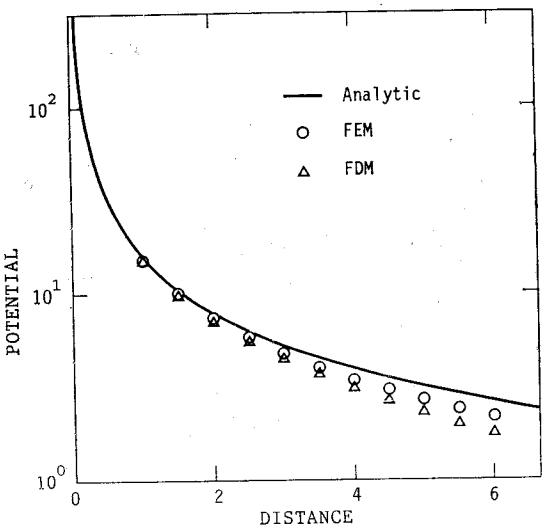

Fig. 3 Surface potentials due to a point source.

shown in Fig. 2.

The width and thickness of each element are small enough to give an accuracy in the apparent resistivity of approximately 4% for the case of 100 Ω·m half-space and a dipole-dipole array. This accuracy is superior to that of the modeling technique using FDM (Kim, 1986) as shown in Fig. 3. The coordinates of nodal points in the FDM are the same as the corresponding coordinates in the FEM.

Although FDM gives more accurate results than FDM, the execution time and core space in FEM are slightly larger than those in FDM. The execution time and core space depend mainly on the dimension of coefficient matrix $[\underline{K}]$ in (7). When one uses a grid of $N\times M$ nodes, the required core spaces are $MN\times(M+1)$ in FDM and $MN\times(M+2)$ in FEM, respectively. Here the size indicated in the bracket is the bandwidth of matrix.

Combining bilinear rectangular and linear triangular elements, one can reduce nodal points in FEM. Fig. 4 shows one of the reduced grids in FEM. This grid has 594 nodal points, and therefore the size of $[\underline{K}]$ is 594×14 (=8316) which is comparable for the grid size in FDM

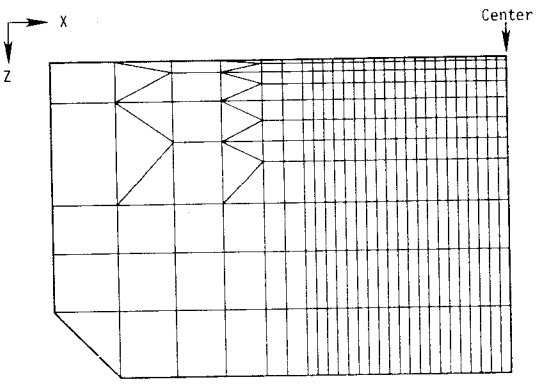

Fig. 4 Left half of a reduced grid with bilinear rectangular and linear triangular elements.

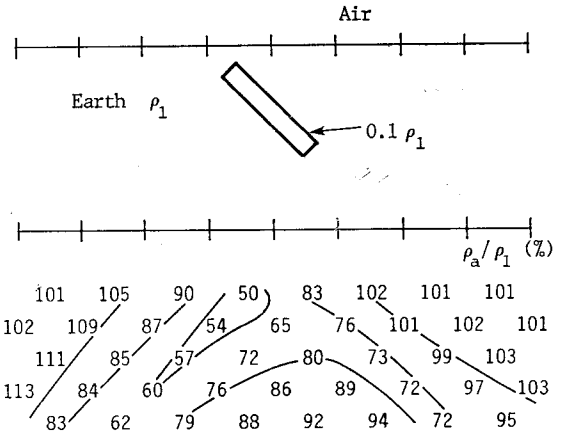

Fig. 5 Pseudo-sectional view of apparent resistivities for the dip model of 45°.

(636×13=8268). When the homogeneous earth of 100Ω·m is simulated using the reduced grid, one can find that its solution has a sufficient accuracy. In fact, in the central equi-spaced nodes, the differences between surface potentials evaluated by FEM's with the grids shown in Fig. 1 and 4 are smaller than 0.035%. This means that with nearly same execution time and core space the FEM gives more accurate results than the FDM.

Another advantages of FEM against FDM are shown in Figs. 5 and 6. The FEM has a greater geometric flexibility to model inhomogeneity (Fig. 5) and topography (Fig. 6) than the FDM. Fig. 5 shows the result for a dip

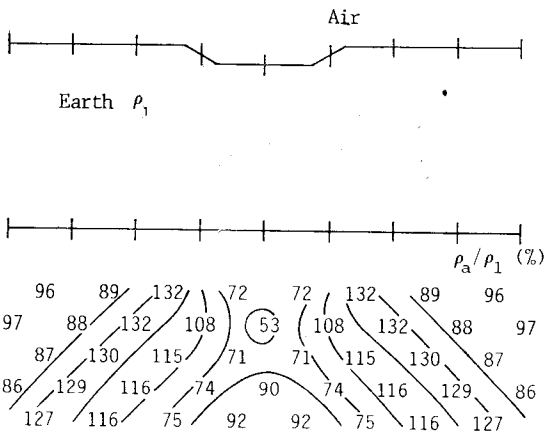

Fig. 6 Pseudo-sectional view of apparent resistivities for the valley model.

model of 45°. From this illustration one can see that a well-known asymmetric pattern appears in the pseudo-section and stronger resistivity anomalies occur in the up-dip side (Coggon, 1973; Kim, 1984). Fig. 6 shows the result for a valley model. From this figure one can find a well-known pattern of anomaly due to the valley (Fox *et al.*, 1980). That is, low resistivity anomalies appear just below the valley and high resistivity anomalies occur in the outsides of the valley.

DISCUSSION AND CONCLUSIONS

In this paper, I developed a finite element modeling technique using both linear triangular and bilinear rectangular elements. The bilinear rectangular element has some useful properties.

Since the interpolation polynomial in the rectanglar element contains a nonlinear term (see (B-1)), the rectangular element can produce more accurate solutions in the interior of the earth than the triangular element. Although the rectangular element requires a specific coordinate as shown in Fig. B1, this property is not inconvenient in the resistivity modeling. Because of this specific coordinate, the rectangular element is more efficient in constructing the matrix equation than the triangular element.

By using only the rectangular elements, the homogeneous earth of 100Ω·m was simulated as shown in Figs. 2 and 3. The coordinates of all nodal points in FEM are the same as the corresponding coordinates in FDM. From Fig. 3, one can find that the FEM produces more accurate results than the FDM.

The geometric flexibility in FEM results from linear triangular elements. This flexibility is useful to reduce nodal points (Fig. 4), to model complex geometry of inhomogeneity (Fig. 5), and to express topography of the earth's surface (Fig. 6).

From the simulation of the homogeneous half-space of 100Ω·m with the reduced grid (Fig. 4), one can find that the FEM gives more accurate results than the FDM with nearly same computer time and core space. This fact may lead another conclusion that with nearly same accuracy FEM is more economic in terms of cost and storage requirements than FDM.

Fox *et al.* (1980) estimated surface topographic effects in resistivity surveys by means of FEM. They simulated the effects of valley and ridge by assuming a fictitious layer between the earth and the air, and by assigning a high resistivity to the fictitious layer. In their model the resistivity contrast between the fictitious region and earth must be less than 10^3 to 10^5, because higher contrasts produce a numerical instability. However, the model in this paper has no fictitious layer and use the natural boundary condition at the earth's surface associated with irregular terrain, and therefore it is free of numerical instability. Another advantage of my approach is that it always has less nodal points in modeling of topography than that of Fox *et al.* (1980).

It is required to specify the boundary conditions at infinitely distant edges. One usually use the boundary condition of either Dirichlet type (the potentials at these edges to be zero) or

Neumann type (the normal derivatives of potential at these deges to be zero). However, since the termination of the lower half-plane at $x=\pm\infty$ and $z=\infty$ is done by extending the meshes far enough away from the sources and conductive inhomogeneities, these two types of boundary conditions have nearly the same effect to numerical solutions in the region of interest. In fact, in the central region of equi-spaced nodes the differences between surface potentials associated with the Dirichlet and the Neumann conditions are less than 0.1% for the homogeneous half-space model of $100\Omega\cdot$m. In the practical point of view, therefore, the Neumann condition is preferable in the resistivity modeling, because the Neumann condition is assigned automatically in FEM so that additional computations associated with boundary conditions can be avoided.

ACKNOWLEDGEMENTS

I wish to thank Drs. C.-E. Baag and Y.Q. Kang for their helpful comments on the manuscript. A part of this study was carried out while I was visiting the University of Hawaii under sponsorship by the Korea Science and Engineering Fodndation.

REFERENCES

Coggon, J.H. (1971) Electromagnetic and electrical modeling by the finite element method. Geophysics, v. 36, p. 132-155.

Coggon, J.H. (1973) A computation of IP electrode arrays. Geophysics, v. 38, p. 737-761.

Conte, S.D. and deBoor, C. (1980) Elementary Numerical Analysis: An Algorithm Approach, 3rd ed. MacGraw-Hill, 432pp.

Fox, R.C., Hohmann, G.W., Killpack, T.J. and Rijo, J. (1980) Topopgraphic effects in resistivity and induced-polarization surveys. Geophysics, v. 45, pp. 75-93.

Kim, H.J. (1986) Resistivity and Induced polarization modeling for arbitrary two-dimensional structures. J. Geol. Soc. Korea, v. 22, p. 366-370.

Sasaki, Y. (1981) Automatic interpretation of resistivity sounding data over two-dimensional structure (I). Butsuri-Tanko (Geophys. Expl.), v. 34, p. 341-350. (in Japanese)

APPENDIX

Linear Triangular Element

The linear triangular element shown in Fig. A1 has straight sides and three nodes, one at each corner. The nodes are labeled counterclockwise: i, j and k. The nodal values of Φ* are ϕ_i, ϕ_j and ϕ_k, and the nodal coordinates are (x_i, z_i), (x_j, z_j) and (x_k, z_k).

The interpolation polynomial is

$$\phi=\beta_1+\beta_2 x+\beta_3 z, \qquad \text{(A-1)}$$

with the nodal conditions

$$\phi=\phi_i \text{ at } x=x_i,\ z=z_i,$$
$$\phi=\phi_j \text{ at } x=x_j,\ z=z_j,$$
$$\phi=\phi_k \text{ at } x=x_k,\ z=z_k. \qquad \text{(A-2)}$$

Substitutions of these conditions into (A-1) produce the matrix equation

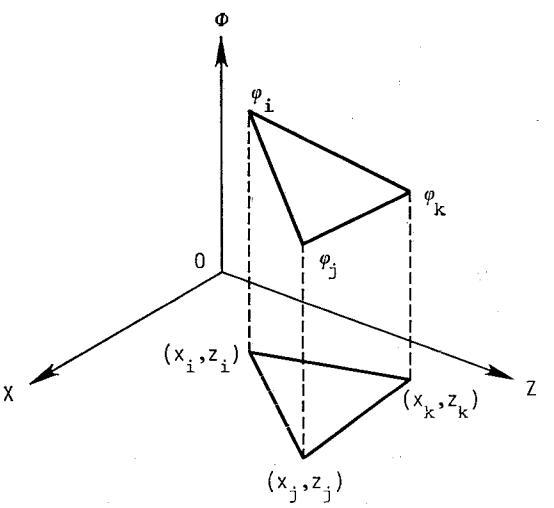

Fig. A1 Parameters for the linear triangular element.

*In this Appendix, the Fourier transformed potential is represented by ϕ instead of Φ.

$$\begin{bmatrix} 1 & x_i & z_i \\ 1 & x_j & z_j \\ 1 & x_k & z_k \end{bmatrix} \begin{bmatrix} \beta_1 \\ \beta_2 \\ \beta_3 \end{bmatrix} = \begin{bmatrix} \phi_i \\ \phi_j \\ \phi_k \end{bmatrix}, \tag{A-3}$$

which yields

$$\begin{bmatrix} \beta_1 \\ \beta_2 \\ \beta_3 \end{bmatrix} = \frac{1}{2A} \begin{bmatrix} a_i & a_j & a_k \\ b_i & b_j & b_k \\ c_i & c_j & c_k \end{bmatrix} \begin{bmatrix} \phi_i \\ \phi_j \\ \phi_k \end{bmatrix}, \tag{A-4}$$

where

$$\begin{aligned} &a_i = k_j z_k - x_k z_j, \quad b_i = z_j - z_k, \quad c_i = x_k - x_j, \\ &a_j = x_k z_i - x_i z_k, \quad b_j = z_k - z_i, \quad c_j = x_i - x_k, \\ &a_k = x_i z_j - x_j z_i, \quad b_k = z_i - z_j, \quad c_k = x_j - x_i, \end{aligned} \tag{A-5}$$

and A is the area of triangle given by

$$2A = \begin{bmatrix} 1 & x_i & z_i \\ 1 & x_j & z_j \\ 1 & x_k & z_k \end{bmatrix}. \tag{A-6}$$

Substitution for β_1, β_2 and β_3 in (A-1) and rearrangement produce an equation for ϕ in terms of three shape functions (N_i, N_j, N_k) and potentials (ϕ_i, ϕ_j, ϕ_k), *i.e.*,

$$\phi = N_i\phi_i + N_j\phi_j + N_k\phi_k, \tag{A-7}$$

where

$$\begin{bmatrix} N_i \\ N_j \\ N_k \end{bmatrix}^T = \frac{1}{2A} \begin{bmatrix} 1 \\ x \\ z \end{bmatrix}^T \begin{bmatrix} a_i & a_j & a_k \\ b_i & b_j & b_k \\ c_i & c_j & c_k \end{bmatrix}. \tag{A-8}$$

The scalar quantity ϕ is related to the nodal values by a set of shape functions that are linear in x and z. This means that the gradients $\partial\phi/\partial x$ and $\partial\phi/\partial z$ are constant within the element. For example,

$$\frac{\partial\phi}{\partial x} = \frac{\partial N_i}{\partial x}\phi_i + \frac{\partial N_j}{\partial x}\phi_j + \frac{\partial N_k}{\partial x}\phi_k, \tag{A-9}$$

but

$$\partial N_n/\partial x = b_n/(2A), \quad n = i, j \text{ and } k. \tag{A-10}$$

Therefore,

$$\partial\phi/\partial x = \beta_2 = (b_i\phi_i + b_j\phi_j + b_k\phi_k)/(2A). \tag{A-11}$$

Similarly,

$$\partial\phi/\partial z = \beta_3 = (c_i\phi_i + c_j\phi_j + c_k\phi_k)/(2A). \tag{A-12}$$

Substitutions of (A-7), (A-11) and (A-12) into (4) produce

$$f = \frac{1}{2}\iint_A \frac{\sigma}{4A^2}\left[(b_i\phi_i + b_j\phi_j + b_k\phi_k)^2 + (c_i\phi_i + c_j\phi_j + c_k\phi_k)^2\right]dA + \frac{1}{2}\iint_A \sigma g^2(N_i\phi_i + N_j\phi_j + N_k\phi_k)^2 dA$$
$$+ \iint_A I\delta(x)\delta(z)(N_i\phi_i + N_j\phi_j + N_k\phi_k)dA.$$

By using the integral formula in area coordinate system

$$\iint_A N_i^a N_j^b N_k^c = \frac{2A(a!b!c!)}{(a+b+c+2)!}, \tag{A-14}$$

the area integrals becomes

$$\iint_A N_i^2 dA = \iint_A N_j^2 dA = \iint_A N_k^2 dA = \frac{A}{6}, \tag{A-15}$$

and

$$\iint_A N_i N_j \, dA = \iint_A N_j N_k \, dA = \iint_A N_k N_i \, dA = \frac{A}{12}. \tag{A-16}$$

Furthermore, by the definition of delta function,

$$\iint_A I\delta(x)\delta(z)dxdz = I, \tag{A-17}$$

and

$$\iint_A xI\delta(x)\delta(z) \, dxdz = \iint_A zI\delta(x)\delta(z) \, dxdz = 0. \tag{A-18}$$

Substitutions of (A-15), (A-16), (A-17) and (A-18) into (A-13) produce

$$f = \frac{\sigma}{8A}\left[(b_i\phi_i + b_j\phi_j + b_k\phi_k)^2 + (c_i\phi_i + c_j\phi_j + c_k\phi_k)^2\right] + \frac{\sigma g^2 A}{12}(\phi_i^2 + \phi_j^2 + \phi_k^2 + \phi_i\phi_j + \phi_j\phi_k + \phi_k\phi_i)$$
$$+ \frac{I}{2A}(a_i\phi_i + a_j\phi_j + a_k\phi_k). \tag{A-19}$$

Applying the minimizing conditions of

$$\partial f/\partial\phi_n = 0, \quad n = i, \ j \text{ and } k, \tag{A-20}$$

to (A-19) yields

$$\frac{\sigma}{4A}\begin{bmatrix} b_i & c_i \\ b_j & c_j \\ b_k & c_k \end{bmatrix}\begin{bmatrix} b_i & c_i \\ b_j & c_j \\ b_k & c_k \end{bmatrix}^T\begin{bmatrix}\phi_i \\ \phi_j \\ \phi_k\end{bmatrix} + \frac{\sigma g^2 A}{12}\begin{bmatrix} 2 & 1 & 1 \\ 1 & 2 & 1 \\ 1 & 1 & 2 \end{bmatrix}\begin{bmatrix}\phi_i \\ \phi_j \\ \phi_k\end{bmatrix} + \frac{I}{2A}\begin{bmatrix} a_i \\ a_k \\ a_k \end{bmatrix} = 0. \tag{A-21}$$

If a point source is located at node i, $x_i = z_i = 0$,

$$a_i = 2A \text{ and } a_j = a_k = 0, \tag{A-22}$$

and the third term in (A-21) becomes $[I, 0, 0]^T$.

Bilinear rectangular element

The bilinear rectangular element shown in Fig. Bl has a length $2b$ and a height $2a$. The nodes are labeled i, j, k and m with node i always at the lower left corner and the nodal values of ϕ are ϕ_i, ϕ_j, ϕ_k and ϕ_m. A local coordinate system where the origin is node i, is set because shape functions are easier to evaluate in this reference frame.

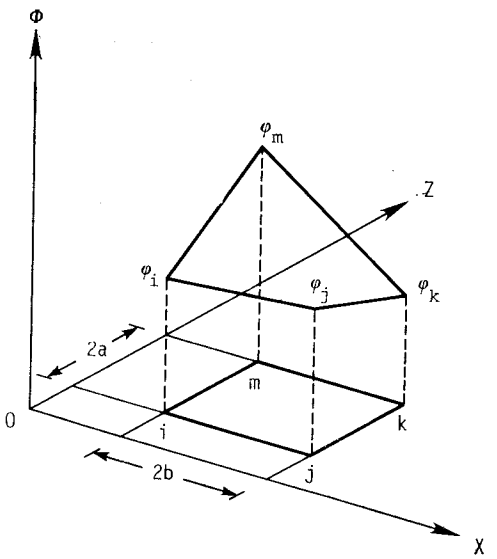

Fig. Bl Parameters for the bilinear rectangular element.

The interpolation polynomial in terms of the local coordinates s and t is

$$\phi = \beta_1 + \beta_2 s + \beta_3 t + \beta_4 st. \tag{B-1}$$

Although the other choices of the interpolation equation (B-1) exist, which would replace the st term by either s^2 or t^2, (B-1) is the most useful because ϕ is linear in s along any line of constant t and linear in t along any line of constant s. Because of these properties, the element is called to be bilinear.

The coefficients β_1, β_2, β_3 and β_4 in (B-1) are obtained by using the nodal values of ϕ and the nodal coordinates, *i.e.*,

$$\begin{pmatrix} 1 & 0 & 0 & 0 \\ 1 & 2b & 0 & 0 \\ 1 & 2b & 2a & 4ab \\ 1 & 0 & 2a & 0 \end{pmatrix} \begin{pmatrix} \beta_1 \\ \beta_2 \\ \beta_3 \\ \beta_4 \end{pmatrix} = \begin{pmatrix} \phi_i \\ \phi_j \\ \phi_k \\ \phi_m \end{pmatrix} \tag{B-2}$$

Solving this gives

$$\begin{pmatrix} \beta_1 \\ \beta_2 \\ \beta_3 \\ \beta_4 \end{pmatrix} = \frac{1}{4ab} \begin{pmatrix} 4ab & 0 & 0 & 0 \\ -2a & 2a & 0 & 0 \\ -2b & 0 & 2b & 0 \\ 1 & -1 & 1 & -1 \end{pmatrix} \begin{pmatrix} \phi_i \\ \phi_j \\ \phi_k \\ \phi_m \end{pmatrix} \tag{B-3}$$

Substitution of (B-3) into (B-1) and rearrangement gives

$$\phi = N_i\phi_i + N_j\phi_j + N_k\phi_k + N_m\phi_m, \tag{B-4}$$

where

$$N_i = (1-s/2b)(1-t/2a), \quad N_j = s/2b(1-t/2a), \quad N_k = st/4ab, \quad N_m = t/2a(1-s/2b). \tag{B-5}$$

Since the (s, t)-coordinate is parallel to the (x, z)-coordinate and a unit length in either s or t is the same as a unit length of x or z,

$$\iint_A f(x, z)\ dxdz = \iint_A f(s, t)\ dsdt. \tag{B-6}$$

The chain rule gives

$$\partial N_n/\partial x = \partial N_n/\partial s, \quad \partial N_n/\partial z = \partial N_n/\partial t, \quad n = i, j, k \text{ and } m. \tag{B-7}$$

Thus the gradients $\partial\phi/\partial x$ and $\partial\phi/\partial z$ are easily obtained as

$$\begin{pmatrix} \dfrac{\partial\phi}{\partial x} \\ \dfrac{\partial\phi}{\partial z} \end{pmatrix} = \frac{1}{A} \begin{bmatrix} -(2a-t) & (2a-t) & t & -t \\ -(2b-s) & -s & s & (2b-s) \end{bmatrix} \begin{pmatrix} \phi_i \\ \phi_j \\ \phi_k \\ \phi_m \end{pmatrix} \tag{B-8}$$

Substitutions of (B-4) and (B-8) into (4) produce

$$f = \frac{\sigma}{2}\iint_A \left[\left(\frac{\partial N_i}{\partial x}\phi_i + \frac{\partial N_j}{\partial x}\phi_j + \frac{\partial N_k}{\partial x}\phi_k + \frac{\partial N_m}{\partial x}\phi_m \right)^2 + \left(\frac{\partial N_i}{\partial z}\phi_i + \frac{\partial N_j}{\partial z}\phi_j + \frac{\partial N_k}{\partial z}\phi_k + \frac{\partial N_m}{\partial z}\phi_m \right)^2 \right] dA$$
$$+ \frac{\sigma g^2}{2}\iint_A (N_i\phi_i + N_j\phi_j + N_k\phi_k + N_m\phi_m)^2\ dA + \iint_A I\delta(x)\delta(z)\ (N_i\phi_i + N_j\phi_j + N_k\phi_k + N_m\phi_m)\ dA. \tag{B-9}$$

Its corresponding area integrals are

$$\iint_A [N_i, N_j, N_k, N_m]\ dA = \frac{A}{4}[1, 1, 1, 1]^T, \tag{B-10}$$

$$\iint_A \begin{pmatrix} N_i^2 & & & * \\ N_iN_j & N_j^2 & & \\ N_iN_k & N_jN_k & N_k^2 & \\ N_iN_m & N_jN_m & N_kN_m & N_m^2 \end{pmatrix} dA = \frac{A}{36} \begin{pmatrix} 4 & 2 & 1 & 2 \\ 2 & 4 & 2 & 1 \\ 1 & 2 & 4 & 2 \\ 2 & 1 & 2 & 4 \end{pmatrix}, \tag{B-11}$$

$$\iint_A \begin{pmatrix} \left(\dfrac{\partial N_i}{\partial x}\right)^2 & & & * \\ \dfrac{\partial N_i}{\partial x}\cdot\dfrac{\partial N_j}{\partial x} & \left(\dfrac{\partial N_j}{\partial x}\right)^2 & & \\ \dfrac{\partial N_i}{\partial x}\cdot\dfrac{\partial N_k}{\partial x} & \dfrac{\partial N_j}{\partial x}\cdot\dfrac{\partial N_k}{\partial x} & \left(\dfrac{\partial N_k}{\partial x}\right)^2 & \\ \dfrac{\partial N_i}{\partial x}\cdot\dfrac{\partial N_m}{\partial x} & \dfrac{\partial N_j}{\partial x}\cdot\dfrac{\partial N_m}{\partial x} & \dfrac{\partial N_k}{\partial x}\cdot\dfrac{\partial N_m}{\partial x} & \left(\dfrac{\partial N_m}{\partial x}\right)^2 \end{pmatrix} dA = \frac{4}{3}a^2 \begin{pmatrix} 2 & -2 & -1 & 1 \\ -2 & 2 & 1 & -1 \\ -1 & 1 & 2 & -2 \\ 1 & -1 & -2 & 2 \end{pmatrix} \tag{B-12}$$

and

$$\iint_A \begin{pmatrix} \left(\frac{\partial N_i}{\partial z}\right)^2 & & * & \\ \frac{\partial N_i}{\partial z}\cdot\frac{\partial N_j}{\partial z} & \left(\frac{\partial N_j}{\partial z}\right)^2 & & \\ \frac{\partial N_i}{\partial z}\cdot\frac{\partial N_k}{\partial z} & \frac{\partial N_j}{\partial z}\cdot\frac{\partial N_k}{\partial z} & \left(\frac{\partial N_k}{\partial z}\right)^2 & \\ \frac{\partial N_i}{\partial z}\cdot\frac{\partial N_m}{\partial z} & \frac{\partial N_j}{\partial z}\cdot\frac{\partial N_m}{\partial z} & \frac{\partial N_k}{\partial z}\cdot\frac{\partial N_m}{\partial z} & \left(\frac{\partial N_m}{\partial z}\right)^2 \end{pmatrix} dA = \frac{4}{3}b^2 \begin{pmatrix} 2 & 1 & -1 & -2 \\ 1 & 2 & -2 & -1 \\ -1 & -2 & 2 & 1 \\ -2 & -1 & 1 & 2 \end{pmatrix} \tag{B-13}$$

Substituting (B-10), (B-11), (B-12) and (B-13) into (B-9) and applying the minimizing condition of f yields finally

$$\frac{\sigma a}{6b}\begin{pmatrix} 2 & -2 & -1 & 1 \\ -2 & 2 & 1 & -1 \\ -1 & 1 & 2 & -2 \\ 1 & -1 & -2 & 2 \end{pmatrix}\begin{pmatrix} \phi_i \\ \phi_j \\ \phi_k \\ \phi_m \end{pmatrix} + \frac{\sigma b}{6a}\begin{pmatrix} 2 & 1 & -1 & -2 \\ 1 & 2 & -2 & -1 \\ -1 & -2 & 2 & 1 \\ -2 & -1 & 1 & 2 \end{pmatrix}\begin{pmatrix} \phi_i \\ \phi_j \\ \phi_k \\ \phi_m \end{pmatrix}$$
$$+\frac{\sigma g^2 ab}{9}\begin{pmatrix} 4 & 2 & 1 & 2 \\ 2 & 4 & 2 & 1 \\ 1 & 2 & 4 & 2 \\ 2 & 1 & 2 & 4 \end{pmatrix}\begin{pmatrix} \phi_i \\ \phi_j \\ \phi_k \\ \phi_m \end{pmatrix} + I\begin{pmatrix} \delta_i \\ \delta_j \\ \delta_k \\ \delta_m \end{pmatrix} = 0 \tag{B-14}$$

where δ_n ($n=i, j, k$ or m) is 1 only if a point source is located at node n and $\delta_n=0$ for the other case.

유한요소법에 의한 2차원 비저항 모델링

김 희 준

요약 : 3각형 및 4각형 요소를 사용한 유한요소법으로 임의의 2차원 비저항 구조에서 점전류원에 대한 전위분포를 구하였다. 이 모델링기술은 종래의 차분법보다 지하의 이상물질이나 지표의 지형을 모델화할 때 보다 더 유연할 뿐만 아니라 보다 더 정확한 수치해를 준다. 또한 이 방법은 해의 정확도에 별 영향없이 격자점을 줄일 수 있기 때문에 계산시간이나 기억용량면에서 경제적이다. 본 논문에서는 이러한 특징을 보여줄 몇 가지 모델에 대한 계산결과를 소개한다.